Electron Density Variation with Incident Power in a Steady State Microwave Discharge

by

Robert E. Terry

Submitted in Partial Fulfillment
of the Requirements for the
Degree of Bachelor of Science

at

Massachusetts Institute of Technology
June , 1968

Signature of Author . Signature redacted . . . . . .
Department of Physics, 17 May 1968

Certified by . . Signature redacted . . . . . .
Thesis Supervisor

Accepted by . . Signature redacted . . . . . .
Chairman, Departmental Committee on Theses

A B S T R A C T

The relation between the electron density and incident power of a helium microwave discharge produced in a waveguide is theoretically and experimentally investigated and found to be linear, consistent with the theoretical treatment of a d.c. helium plasma column by Ecker and Zöller (ref. 7). The wave equation is solved for a plane wave incident on a plasma slab with a parabolic density profile in the direction of propagation and compared with behavior of a uniform plasma slab. The experimental behavior of the cylindircal plasma column is found to be consistent with the above theoretical treatments.

A C K N O W L E D G E M E N T S

The author wishes to express his appreciation for the help and cooperation of all those in the plasma group,: especially to Prof. J. C. Ingraham for much patience, help, and wise council, to the Research Laboratory of Electronics and the Atomic Energy Commission for sponsoring this work, to J. J. McCarthy for aid and advice in instrumentation, to L. W. Ryan and his staff for prompt and conscientious maintenance on the vacuum system, and to L. P. Mix for help in the theoretical calculations, without whose help this work would have been impossible or severly hampered.

TABLE OF CONTENTS

I N T R O D U C T I O N

The object of this thesis is to investigate the relation between the electron density and the magnitude of the incident electric field in a steady state microwave discharge in He gas containing a small amount of Hg impurity. The general problem of microwave breakdown has been well covered in previous work (ref. 1, p. 165); and, while the steady state operation of the discharge has been discussed (ref. 2,3,4), the specific problem of the variation of electron density with the strength of the incident electric field has not been treated explicitly.

It is well known that, after breakdown occurs and the electron density builds up from the free diffusion limit of breakdown to the ambipolar diffusion limit of higher density plasma, the electric field strength required to sustain the discharge becomes progressively less than that required for breakdown. What happens to the electron density and the field inside the plasma as the incident field strength is increased on a plasma already in the ambipolar diffusion limit is essentially the quest of this investigation.

The theoretical treatment of the problem is considered in two aspects: the interaction of the incident electromagnetic fields with the plasma, in regard to obtaining

the fields inside the plasma as a function of the electron density given the incident fields; and the energy and particle conservation within the discharge with regard to relating the energy and particle transport to the field inside the plasma.

The experimental techniques employed are well known and will be discussed in detail in later sections; basically, the procedure was first to observe the microwave power absorbed by the plasma and its total light output as a function of the incident power for the case of a discharge tube inserted into a section of rectangular wave guide and then using a resonant cavity and the same discharge tube to correlate the light output with the electron density as measured by the shift in resonant frequency of a given cavity mode as the plasma density is increased in the cavity.

The results of these experiments indicate that, for the waveguide discharge, the plasma density increases linearly with the incident power. The gas temperature and its distrubution is found to play an important role in determining the density and temperature of the electrons.

II. Theory of Discharge Operation

II.-1 The Particle and Energy Balance:

In a steady state discharge the particle and energy densities must be independent of time; this requires that there exist a local detailed balance between the particle production (ionization) rate and the particle loss (diffusion) rate and between the energy absorbed by the electrons (from the driving field) and the energy loss rate (due to collision with the gas atoms). The particle loss and production rates and the energy transport and absorbtion are functions of position, in general, within the discharge in that they depend on the gas atom temperature, which can be taken as equal to the ion temperature.

If we assume that all the energy absorbed by the electrons is eventually lost to the energy of the gas atoms and ions via collision, the basic energy balance which must hold locally at all points in the discharge is given by:

$$[1] \quad \frac{e^2 E_o^2}{2 m_e} \cdot \frac{\nu_m}{\nu_m^2 + \omega^2} = \frac{3}{2} k \left(T_e - T_g \right) \gamma \nu_m$$

ν_m is the electron-gas atom collision frequency; m_e, T_e, and T_g are the electron mass, temperature and gas atom temperature respectively. The left hand side is the average energy absorbed per second per electron from a time dependent driving field $\vec{E} \sim e^{-i\omega t}$, $\frac{\overline{\vec{J} \cdot \vec{E}}}{n_e}$ (ref. 5); the right hand side, the energy lost via collision per second per electron, where γ is the average fractional energy loss per collision (ref. 6). This equation then prescribes a local contraint on T_e, T_g and E_o which is required to run the discharge in a steady state, independent of the local electron density.

For the case of a d.c. discharge equation [1] is much the same, except that the left hand side loses the factor $\nu_m / (\nu_m^2 + \omega^2) \cdot 2$ which comes from the time average of $\vec{J} \cdot \vec{E}$ and is now written:

[2] $\frac{e^2 E_o^2}{m_e \nu_m} = \frac{3}{2} k (T_e - T_g) \gamma \nu_m$. Under this assumption, coupled with that of ambipolar diffusion and negligible energy lost to radiation, the d.c. discharge has been treated in detail by G. Ecker and O. Zöller (ref. 7). In this treatment the transport equations for particle and energy conservation as solved for T_g and n_e (the electron density) as functions of position and the macroscopic

parameters E_o (inside the plasma), p, the pressure, and R, the plasma radius, for a cylindrical, axially uniform and azimuthally symmetric plasma. The field E_o is taken as constant and equation [2] is used to eliminate T_e from the transport equations, leaving only T_g and n_e as unknowns. The simplified equations which are finally solved are:

[3] Particle transport:

$$\frac{1}{r}\frac{d}{dr}\left(r\, D[T_g]\,\frac{dn_e}{dr}\right) + \frac{1}{r}\frac{d}{dr}\left(r\, n_e\, D[T_g]\,\frac{d}{dr}\ln T_g\right) + \alpha[T_g] = 0$$

[4] Energy transport:

$$\frac{1}{r}\frac{d}{dr}\left(r\,\lambda[T_g]\,\frac{dT_g}{dr}\right) + e E_o^2\,\mu_e[T_g]\,n_e = 0$$

where: $D[T_g]$ = local ambipolar diffusion coefficient

$\lambda[T_g]$ = local gas heat conductivity

$\mu_e[T_g]$ = local electron mobility

and $\alpha[T_g]$ = local ionization rate. The solution of [3] and [4] is required to satisfy [2] at all points. This solution is presented in various ways, specifically: $n_e/n_{e,center}$ vs. $\frac{r}{R}$, for various Ip; $n_{e,center}$ vs. Ip, for various Rp; T_g vs. r/R, for various Ip; $T_{g,center}$ vs. Ip, for various Rp; RE_o vs. Ip for various Rp, where I is the axial current through the discharge.

In order to apply this treatment approximately to an a.c. discharge the first step is to replace E_o^2 by its r.m.s. value $\frac{E_o^2}{2}$ for the time dependent driving field, $E_o\, e^{-i\omega t}$. This will in no way affect the form of the solutions of [3] and [4] since E_o is a variable parameter in this treatment. The only real question arises with respect to the second term of equation [4], which contains the d.c. mobility $\mu_e[T_g]$. If this is replaced by the a.c. mobility $\mu_e \frac{\nu_m^2}{\nu_m^2+\omega^2}$ it must be assumed that $\nu_m^2 >> \omega^2$ in order to preserve the same temperature dependence for this term, equation [4]. In this investigation the cases of interest are for $\nu_m^2 \geqq 8\omega^2$, (with ν_m evaluated at room temperature) so the approximation is somewhat valid.

The rationale of the application is quite straightforward. The solution of Ecker and Zöller yields a roughly parabolic variation of gas temperature with radius and a progressively flattened electron density profile with increasing power absorbed. Using the given curves it is possible to generate plots of $\Delta T = T_{g,center} - T_{g,wall}$ as a function of P' and also the variation of $n_{e,center}$ as a function of P', where P' is the power absorbed per unit length along the axis and is given by IE_o, since the product R_p is known for the experimental set-up used. Both of these plots are reasonably linear and are shown in Fig. 1

and 2. The ΔT vs. P' seems best fitted by $\Delta T = 70\, P'\ (^{\circ}K)$ and the $n_{e,center}$ vs. P' is, to a good approximation given by $n_{e,c} = c(P')^{1.1}$.

Fig. 1 (from Ecker and Zöller)

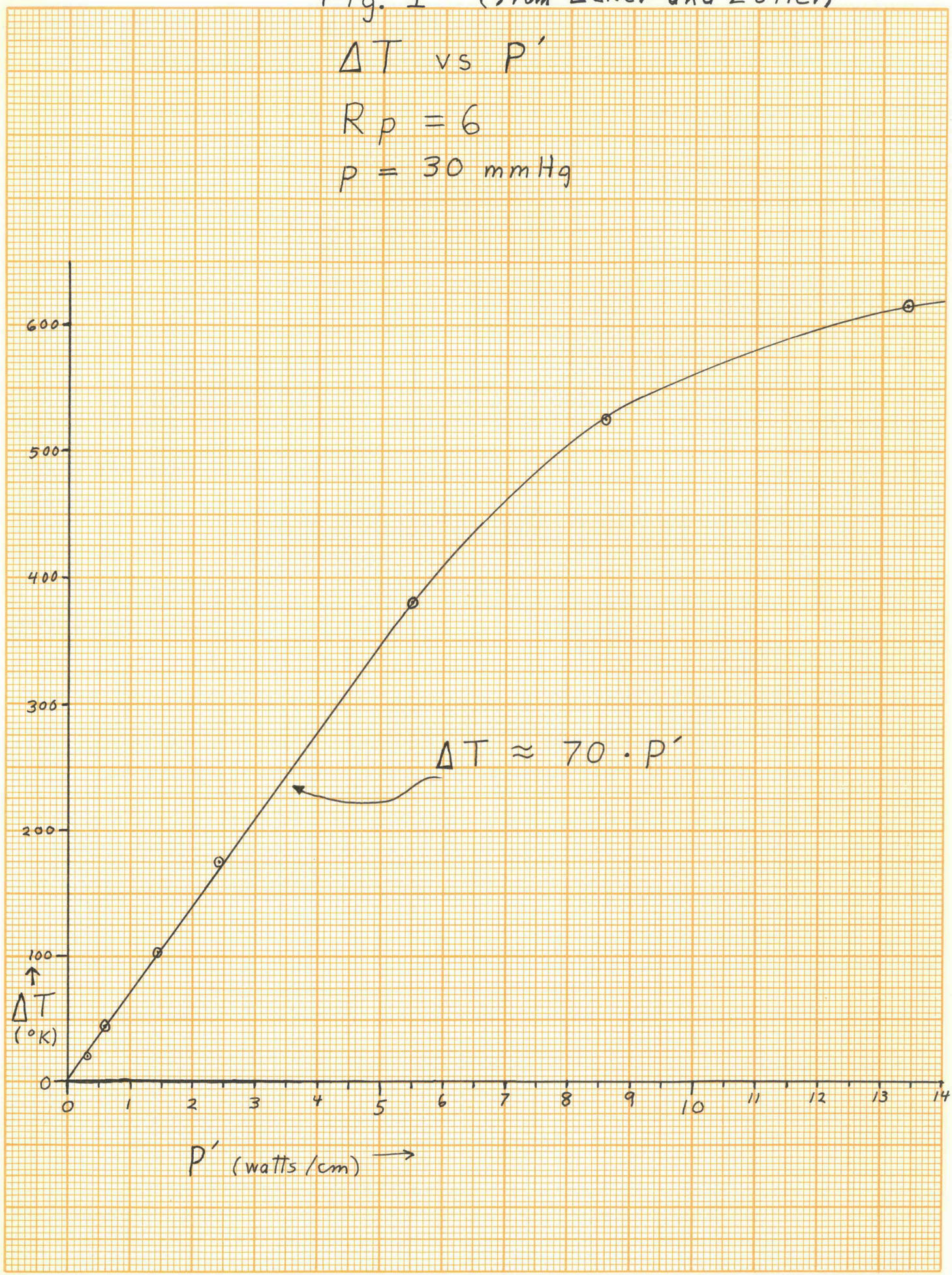

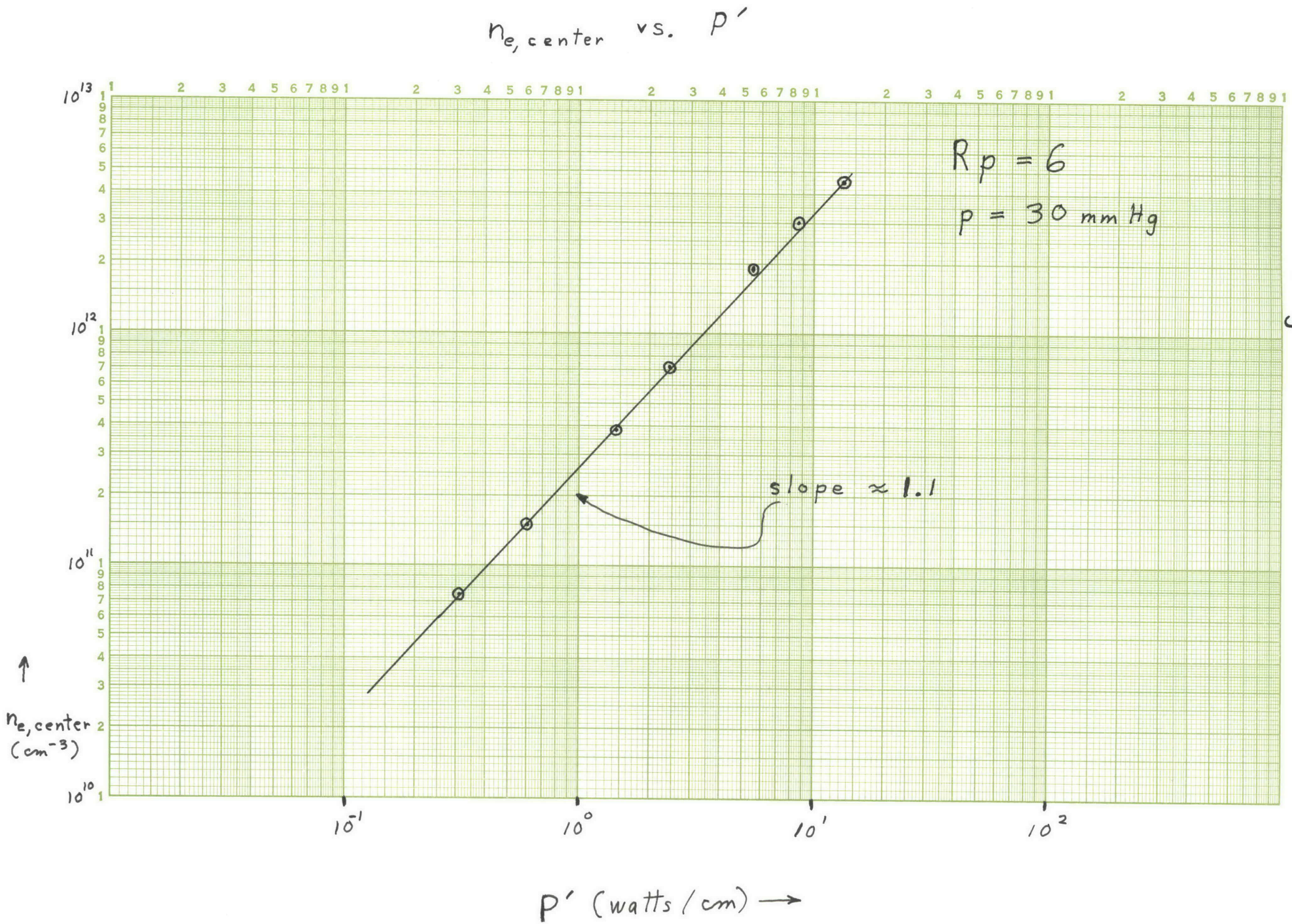

Fig. 2 (from Ecker and Zöller)

II.-2 The Electromagnetic Problem:

In this section the interaction of a plane electromagnetic wave with two possible electron density profiles, uniform and parabolic, will be treated with regard to calculating the magnitude of the electric field as a function of position and electron density within the plasma for a known incident field.

The complex dielectric coefficient, $\breve{K}$, for a plasma of spatial distribution, $n_e = n_e(x,y,z)$, is given by:

$$[5] \quad \breve{K} = 1 - \frac{\omega_p^2(x,y,z)}{\omega^2 + \nu_m^2}\left(1 - i\,\frac{\nu_m}{\omega}\right) \qquad \text{(ref. 8, p. 6)}$$

with $\omega_p^2(x,y,z) = \frac{e^2}{m_e \epsilon_0}\, n_e(x,y,z)$, in MKS units,

ω = angular frequency of the incident field, $E \sim e^{-i\omega t}$

and ν_m = collision frequency for momentum transfer between electrons and gas atoms, a function of the local gas atom density.

In terms of $\breve{K}$, the wave equation for $\vec{E}$ is

$$[6] \quad \nabla^2 \vec{E} + k^2 \breve{K}\, \vec{E} = -\vec{\nabla}\left[\frac{\vec{\nabla}\breve{K} \cdot \vec{E}}{\breve{K}}\right] \qquad \text{(ref. 9, p. 44)}$$

and, if there are no gradients of $\breve{K}$ along the direction of the incident $\vec{E}$, then $\vec{\nabla}\breve{K} \cdot \vec{E} = 0$, and the wave equation is

separable for some forms of $\breve{K}(x,y,z)$ and suitable coordinate systems.

Applying this wave equation to a plasma slab of thickness, L, with a parabolic electron density profile along the direction of propagation of the normally incident plane wave, $\vec{E}_z = \vec{E}_{zo}\, e^{i(k_o x - \omega t)}$, and independent of position in directions perpendicular to the direction of propagation yields:

$$[7] \qquad \frac{d^2 \vec{E}_z(x)}{dx^2} + k_o^2\, \breve{K}(x)\, \vec{E}_z(x) = 0$$

as the simplified wave equation with $\vec{E}_y = \vec{E}_x = 0$. The parabolic density profile can be written as $\omega_p^2(x) = \omega_{po}^2 \frac{x(L-x)}{(L/2)^2}$; substituting this and the change of variable $\eta = k_o x$ into equation 7 yields:

$$[8] \qquad \eta^2 \frac{d^2 E_z(\eta)}{d\eta^2} + \left\{ \eta^2 - \frac{4\alpha}{\eta_L}\eta^3 + \frac{4\alpha}{\eta_L^2}\eta^4 \right\} E_z(\eta) = 0$$

where: $\eta_L = k_o L$, $\alpha = \frac{\omega_{po}^2}{\nu_m^2 + \omega^2}\left(1 - i\,\nu_m/\omega\right)$ as the equation determining $E_z(\eta)$ within the discharge.

The substitution of a power series approximation for E_z, namely $E_z = E_{oz} \sum_{n=0}^{\infty} a_n \eta^n$, and the requirement that the following boundary conditions, expressing continuity

of E_z and H_y at the incident and transmitted boundaries, hold:

[9]
$$E_z: \; 1 + R = E_z(\eta = 0) \qquad T e^{i\eta_L} = E_z(\eta = \eta_L)$$

$$H_y: \; 1 - R = -i \frac{d}{d\eta} E_z(\eta = 0) \qquad T e^{i\eta_L} = -i \frac{d}{d\eta} E_z(\eta = \eta_L)$$

where $R = E_{Reflected} / E_{oz}$, $T = E_{Transmitted} / E_{oz}$

yields to order η^2 the following expressions for the real and imaginary parts of the field $\frac{\vec{E}_z(\eta)}{E_{oz}}$:

[10]
$$Re\left[\frac{E_z(\eta)}{E_{oz}}\right] = 1 + \frac{\beta \eta_L A}{C} + \frac{\beta \eta_L B}{C} \cdot \eta - \left(1 + \frac{\beta \eta_L A}{C}\right) \eta^2/2 + \left[\frac{2\beta^2 B \gamma}{3C} + \left(1 + \frac{\beta \eta_L A}{C}\right) \frac{2\beta}{3\eta_L}\right] \eta^3 - \left[\frac{\gamma \beta^2 B}{3\eta_L C} - \left(1 + \frac{\beta \eta_L A}{C}\right) \frac{\beta}{3\eta_L^2}\right] \eta^4$$

[11]
$$Im\left[\frac{E_z(\eta)}{E_{oz}}\right] = \frac{\beta \eta_L B}{C} + \left(1 - \frac{\beta \eta_L A}{C}\right) \cdot \eta - \left(\frac{\beta \eta_L B}{C}\right) \eta^2/2 + \left[\frac{2\beta^2 B}{3C} - \left(1 + \frac{\beta \eta_L A}{C}\right) \frac{2\beta\gamma}{3\eta_L}\right] \eta^3 - \left[\frac{\beta^2 B}{3\eta_L C} - \left(1 + \frac{\beta \eta_L A}{C}\right) \frac{\beta\gamma}{3\eta_L^2}\right] \eta^4$$

where: $\beta = \dfrac{\omega_{po}^2}{\nu_m^2 + \omega^2}$, $\gamma = \nu_m / \omega$

and $A = (3\eta_L - \beta\eta_L + \beta\gamma\eta_L^2) - \gamma(3 + \beta\gamma\eta_L - \eta_L^2(3/2 + \beta))$

$B = (3\eta_L - \beta\eta_L + \beta\gamma\eta_L^2)\cdot(-\gamma) - (3 + \beta\gamma\eta_L - \eta_L^2(3/2+\beta))$

$C = (3\eta_L - \beta\eta_L + \beta\gamma\eta_L^2)^2 + (3 + \beta\gamma\eta_L - \eta_L^2(3/2+\beta))^2$.

These expressions have been evaluated for several values of the parameters γ, β, and η with $\eta_L = .2$ and the results are shown in the following plots, Figs. 3 and 4.

For the uniform plasma slab of thickness, L, the fields inside can be determined exactly simply by matching boundary conditions, as in the previous case, between a plane wave $E_z = E_{oz} e^{i(k_o x - \omega t)} + E_{Rz} e^{-i(k_o x + \omega t)}$ incident (E_{oz}) on and reflected (E_{Rz}) from the plasma; a similar wave within the plasma, $\mathcal{E}_{o+} e^{i(\check{k}x - \omega t)} + \mathcal{E}_{o-} e^{-i(\check{k}x + \omega t)}$, with components traveling in the positive and negative $\hat{x}$ directions, and the complex wave number, $\check{k} = k_o(\alpha + i\beta)$; and a transmitted wave $E_z = E_{Tz} e^{i(k_o x - \omega t)}$ on the other side of the slab. The components of the complex wave number $\check{k}$ are given by:

[12] $$\alpha = \frac{1}{\sqrt{2}} \sqrt{\sqrt{\gamma^2 + \delta^2\eta^2} + \gamma}$$

$$\beta = \frac{1}{\sqrt{2}} \sqrt{\sqrt{\gamma^2 + \delta^2\eta^2} - \gamma}$$

with $\gamma = 1 - \eta$, $\eta = \dfrac{\omega_p^2}{\nu_m^2 + \omega^2}$, $\delta = \dfrac{\nu_m}{\omega}$

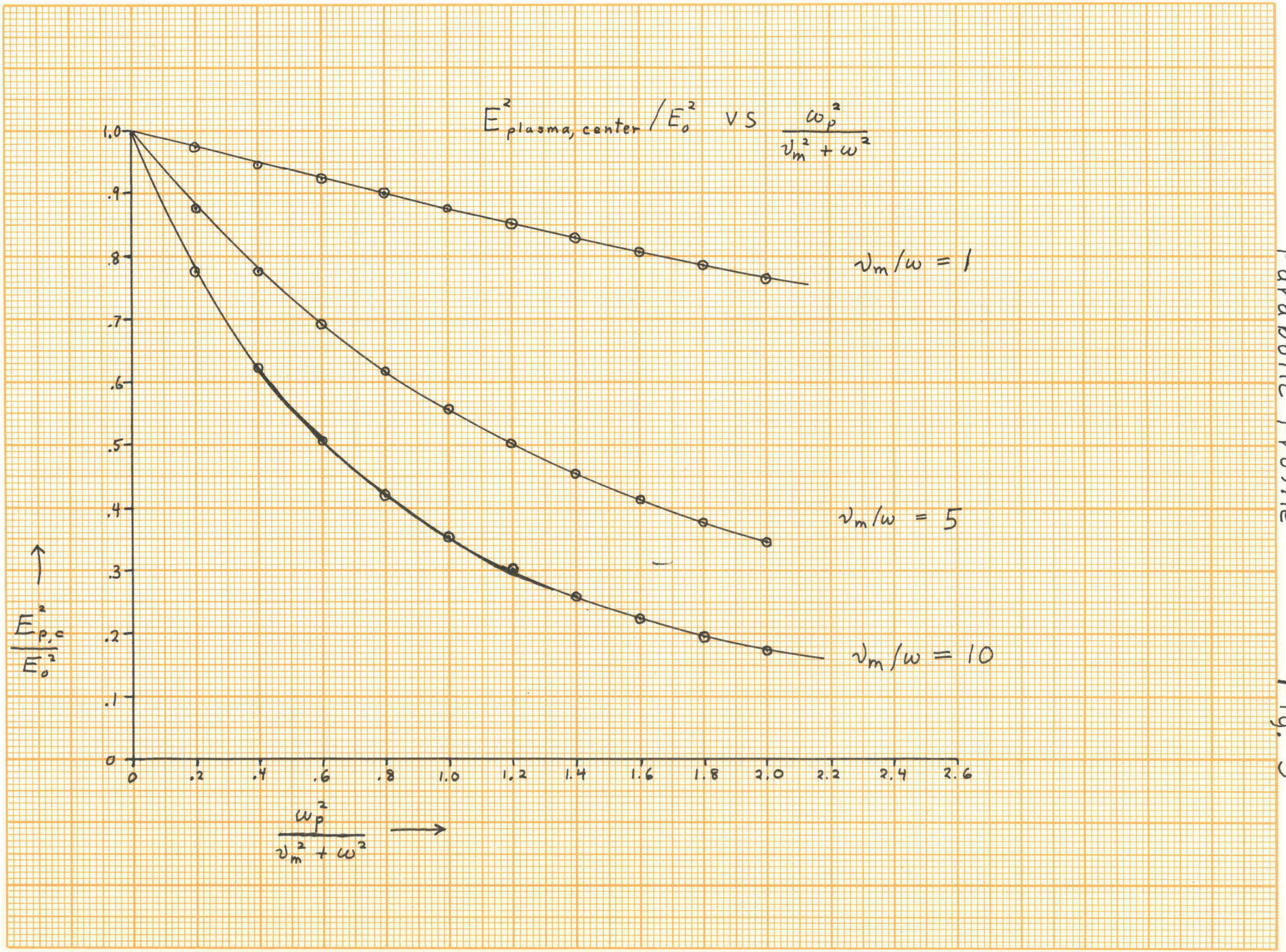

Parabolic Profile Fig. 3

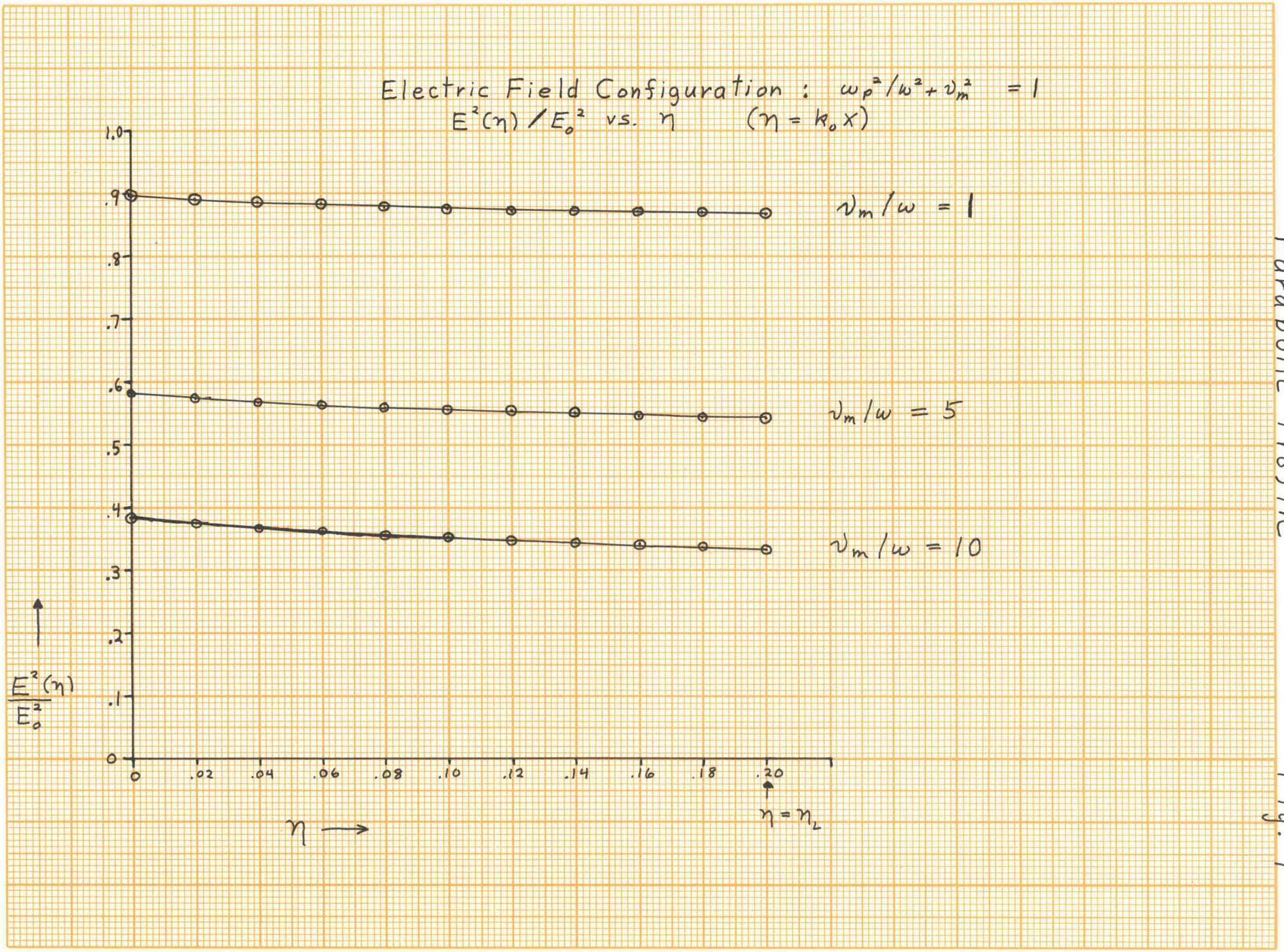

Parabolic Profile Fig. 4

ω_p^2 being independent of position inside the plasma and 0 outside. The equations expressing the boundary conditions at the incident and transmitted faces respectively are:

[13] $X = 0$

continuity of E_z : $E_{zo} + E_{zR} = \mathcal{E}_{o+} + \mathcal{E}_{o-}$

continuity of H_y : $E_{zo} - E_{zR} = (\alpha + i\beta)(\mathcal{E}_{o+} - \mathcal{E}_{o-})$

$X = L$

continuity of E_z : $\mathcal{E}_{o+} e^{i\breve{k}L} + \mathcal{E}_{o-} e^{-i\breve{k}L} = E_{TZ} e^{ik_o L}$

continuity of H_y : $(\alpha + i\beta)\left[\mathcal{E}_{o+} e^{i\breve{k}L} + \mathcal{E}_{o-} e^{-i\breve{k}L}\right] = E_{TZ} e^{ik_o L}$.

Solving these equations for $\mathcal{E}_{o+}$ and $\mathcal{E}_{o-}$ generates the following expressions:

[14] $$\mathcal{E}_{o+} = \frac{2E_{zo}[1+\alpha+i\beta]}{[1+\alpha+i\beta]^2 - e^{2i\breve{k}L}[1-\alpha-i\beta]^2}$$

$$\mathcal{E}_{o-} = \frac{2E_{zo}[1-\alpha-i\beta]}{[1-\alpha-i\beta]^2 - e^{-2i\breve{k}L}[1+\alpha+i\beta]^2}$$

and the resulting expression for the total E field at any point in the plasma is:

[15] $$E_z(x) = \mathcal{E}_{o+} e^{i\breve{k}x} + \mathcal{E}_{o-} e^{-i\breve{k}x}.$$

This expression has been evaluated for various values of

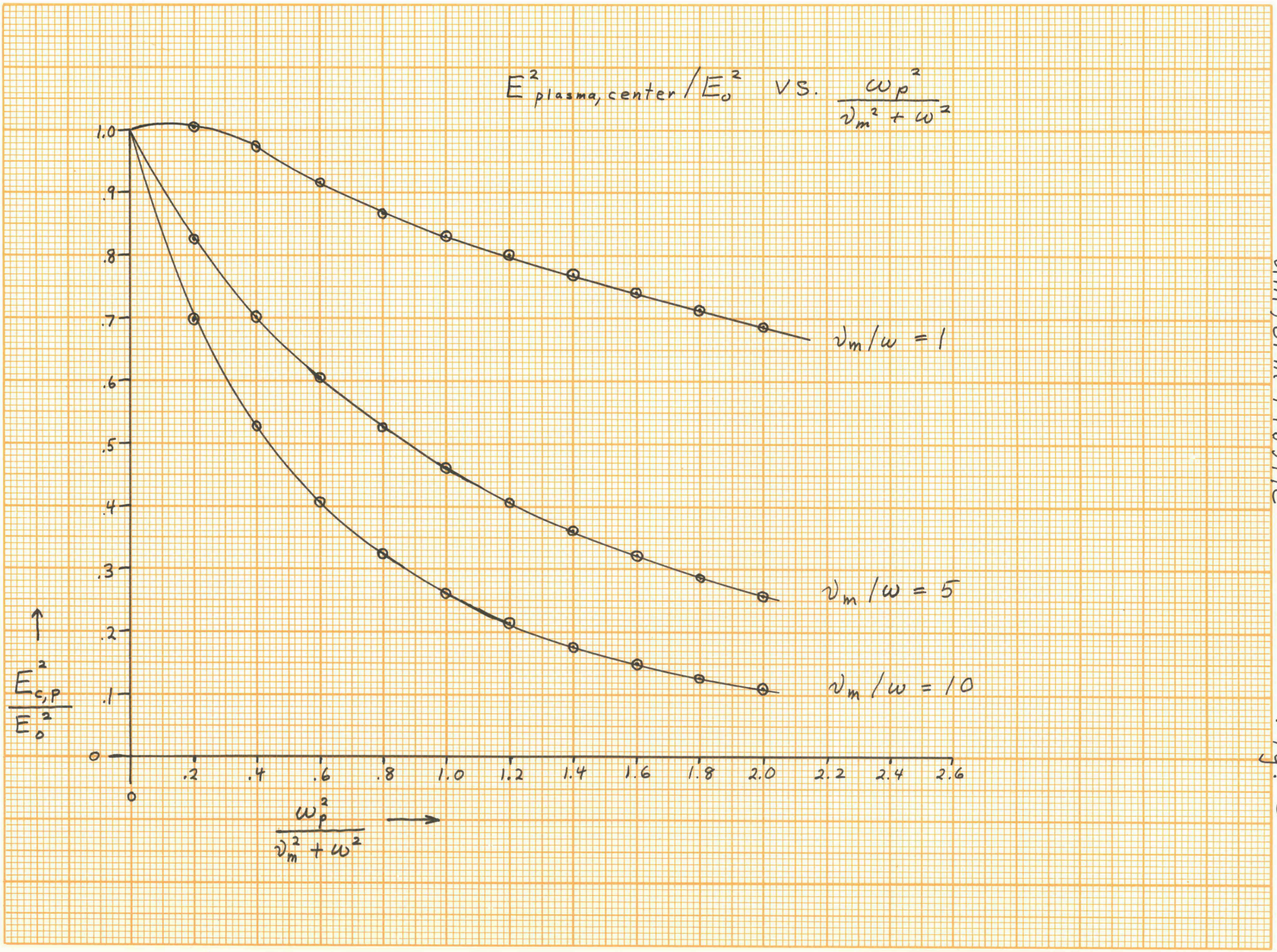

Uniform Profile

Fig. 5

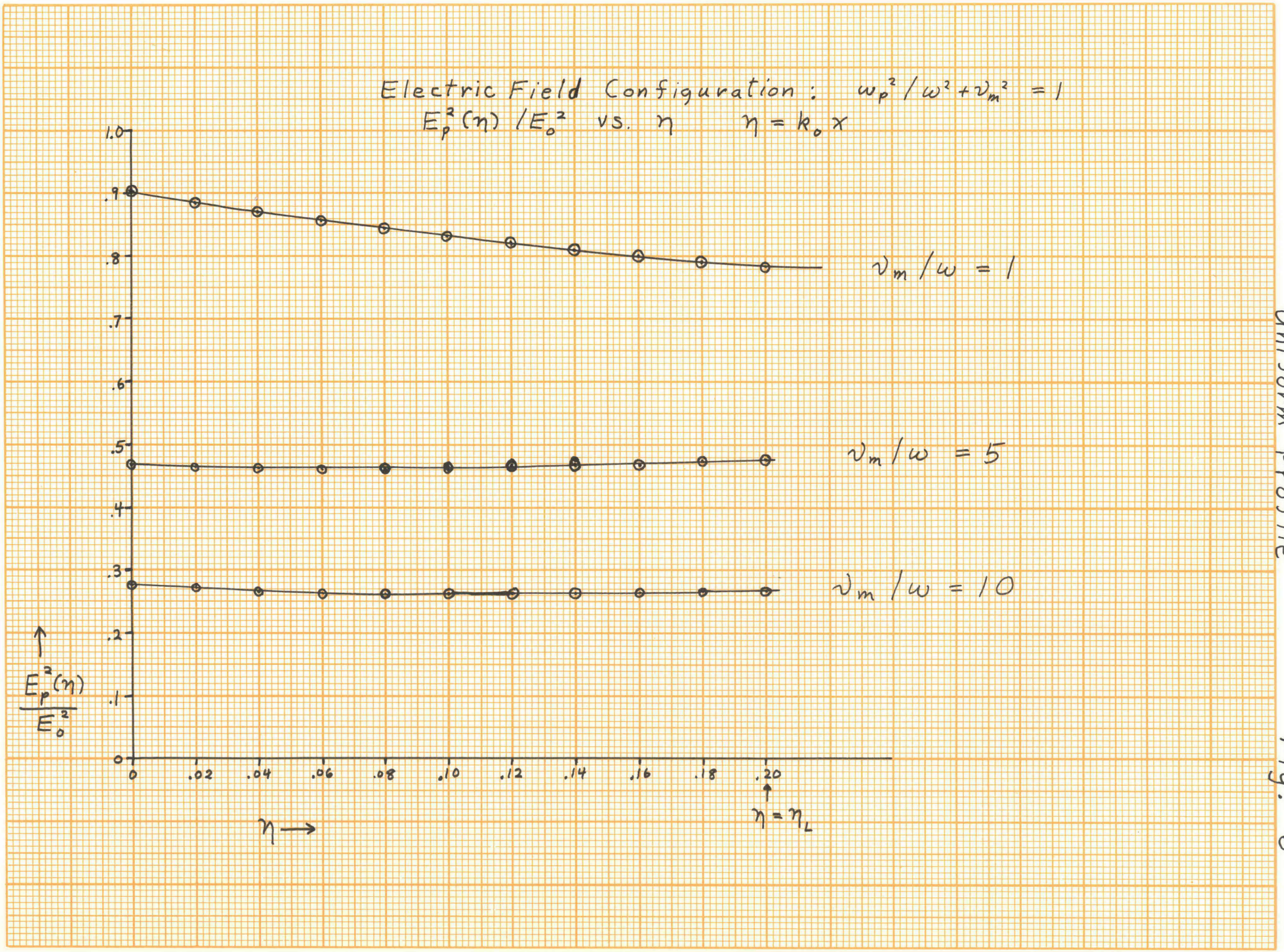

Uniform Profile

Fig. 6

$k_0 x$, η and δ with $k_0 L = .2$, and the resulting plots are shown in Fig. 5 and 6.

In order to apply this theory to the case of a discharge tube in a waveguide with the tube axis along the incident $\vec{E}$, it must be assumed that there are no plasma density gradients or temperature gradients along the axis of the tube and that the plasma dimensions are small compared with those of the waveguide and the wavelength of the radiation incident on the plasma. It is clear from the plots of these results that the uniform plasma with $\omega_p^2 = \omega_{po}^2$, of the parabolic case, will attenuate the radiation more efficiently than a non-uniform density such as the parabolic profile. This is to be expected since the uniform plasma absorbs strongly over a longer path length than a plasma with a peaked profile. For large values of ν_m/ω and/or large values of $\omega_p^2/(\nu_m^2 + \omega^2)$ both the uniform and parabolic profiles yield an inverse proportionality between $E_z^2(x)/E_{oz}^2$ and n_e, as is shown in Fig. 7 and 8. For these ranges of the parameters the square of the ratio of electric field inside the plasma to the incident electric field is roughly inversely proportional to the electron density. Furthermore, the inverse proportionality holds for all values of X inside the discharge for n_e taken as $n_{e,center}$ i.e. the field configuration inside the plasma does not change much as the density increases.

$E^2_{plasma,\,center} / E_o^2$ vs $\left[\frac{\omega_p^2}{\nu_m^2 + \omega^2}\right]^{-1}$

Note: in experiment $\nu_m/\omega \approx 2.8$, $\left[\frac{\omega_p^2}{\nu_m^2+\omega^2}\right]^{-1} \approx .1430$

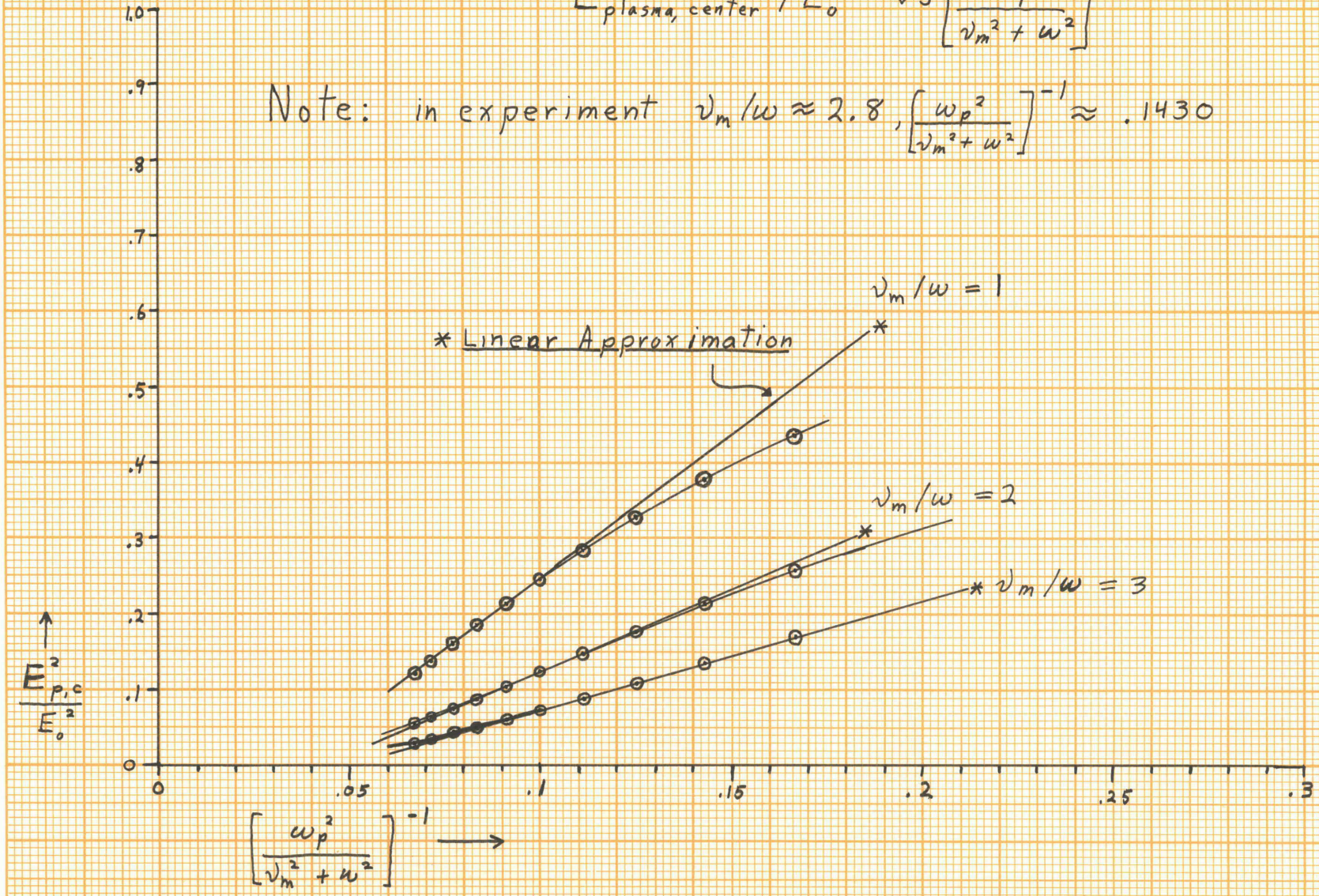

Parabolic Profile

Fig. 7

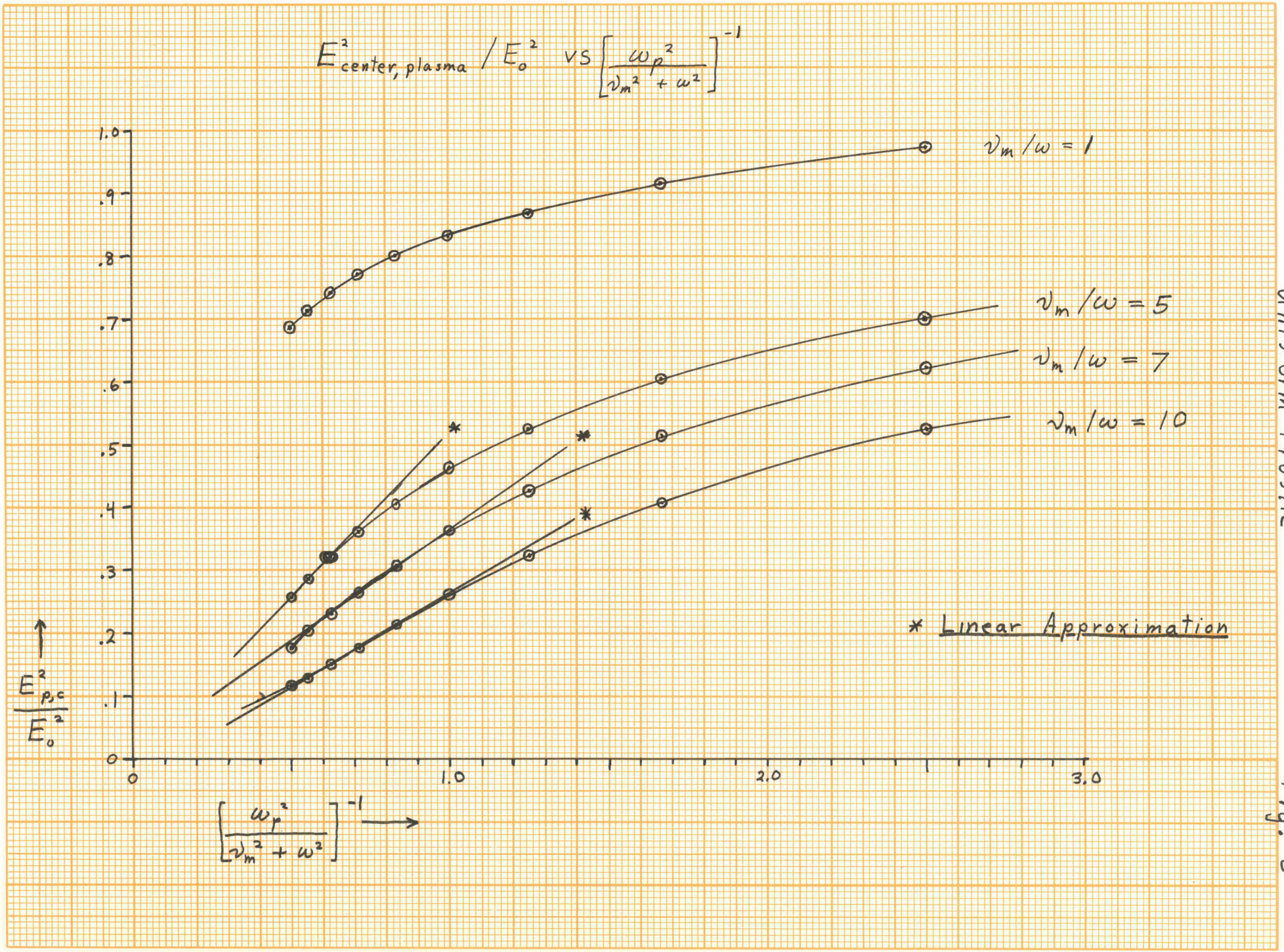

Uniform profile

Fig. 8

II.-3 Calculation of Electron Density from Cavity Frequency Shifts

In general for a cylindrical resonant cavity of radius R_o, with a coaxially inserted discharge tube of radius R, the fractional frequency shift, $\frac{\Delta f}{f_o}$, for a mode of frequency f_o in the absence of any plasma is given by:

$$[16] \quad \frac{\Delta f}{f_o} = -\frac{1}{2} \frac{\int [\mu_R^2 - 1] \vec{E}_o \cdot \vec{E}_o \, dv}{\int \vec{E}_o \cdot \vec{E}_o \, dv} \qquad \text{(ref.10,p.8)}$$

where $\mu_R^2 = 1 - \frac{\omega_p^2(r)}{\omega^2 + \nu_m^2(r)}$, the real part of the plasma index of refraction. The integration is taken over the cavity volume and $\vec{E}_o$ is the field configuration in the absence of plasma for the mode of interest; this constitutes, then, a first order perturbation on the cavity fields. Substitution of the expression for μ_R^2 into [16] yields:

$$[17] \quad \frac{\Delta f}{f_o} = \frac{1}{2} \frac{\int \frac{\omega_p^2(r)}{\omega^2 + \nu_m^2(r)} \vec{E}_o \cdot \vec{E}_o \, dv}{\int \vec{E}_o \cdot \vec{E}_o \, dv} \; .$$

The radial dependence of ν_m occurs due to the gas temperature dependence of ν_m, $\nu_m = c\, T_g^{-1}$. The mode of interest here is the TE_{011}, for which $E_\theta(r) \sim r$; thus this mode is sensitive to the profile functions for large r,

where $\nu_m \approx \nu_{m,wall} = \nu_m(T_{g,wall})$ and thus ν_m is replaced by $\nu_{m,wall}$ in equation [17] and the evaluation can be taken directly from (ref. 10, p. 11) for appropriate values of R and R_o. This yields:

$$[18] \qquad \frac{\Delta f}{f_o} = \frac{1}{2} \frac{\omega_{po}^2}{\nu_{m,wall}^2 + \omega^2} \eta_{oll}$$

where ω_{po}^2 is the value $\omega_p^2(r=0)$ and η_{oll} is found from (10) for either a Bessel function, $J_o(2.4\,r/R)$, or a uniform profile.

III. Experimental Techniques and Procedures

For these experiments the equipment consisted of a microwave driving circuit to produce the discharge, a diagnostic circuit to detect and measure the cavity frequency shifts, and a light monitor. The plasma was produced by either inserting the discharge tube through a section of C-band waveguide, as shown in Fig. 9; or mounting it axially in a high Q cylindrical resonant cavity, as shown in Fig. 10. The cavity was made of silver plated brass with the inner surfaces polished and, for the TM_{010} and TE_{011} modes were 4.0 Gc and 9.28 Gc, respectively. Coupling to the various cavity modes was accomplished with coaxial loops inserted into the cavity.

The driving circuit is shown in Fig. 11 for the waveguide discharge and Fig. 12 shows the modifications involved in switching over to a cavity discharge. For both types of discharge the magnetron power supply was set to maximum output and the power divider used to control the power incident on the plasma. The various directional couplers and variable attenuators shown were all calibrated separately at 4.3 Gc with a P.R.D. type G-101 calibrated attenuator and a General Microwave, 454A power meter and then combined into 50db attenuation units so that a reasonably accurate

Waveguide Discharge

Fig. 9

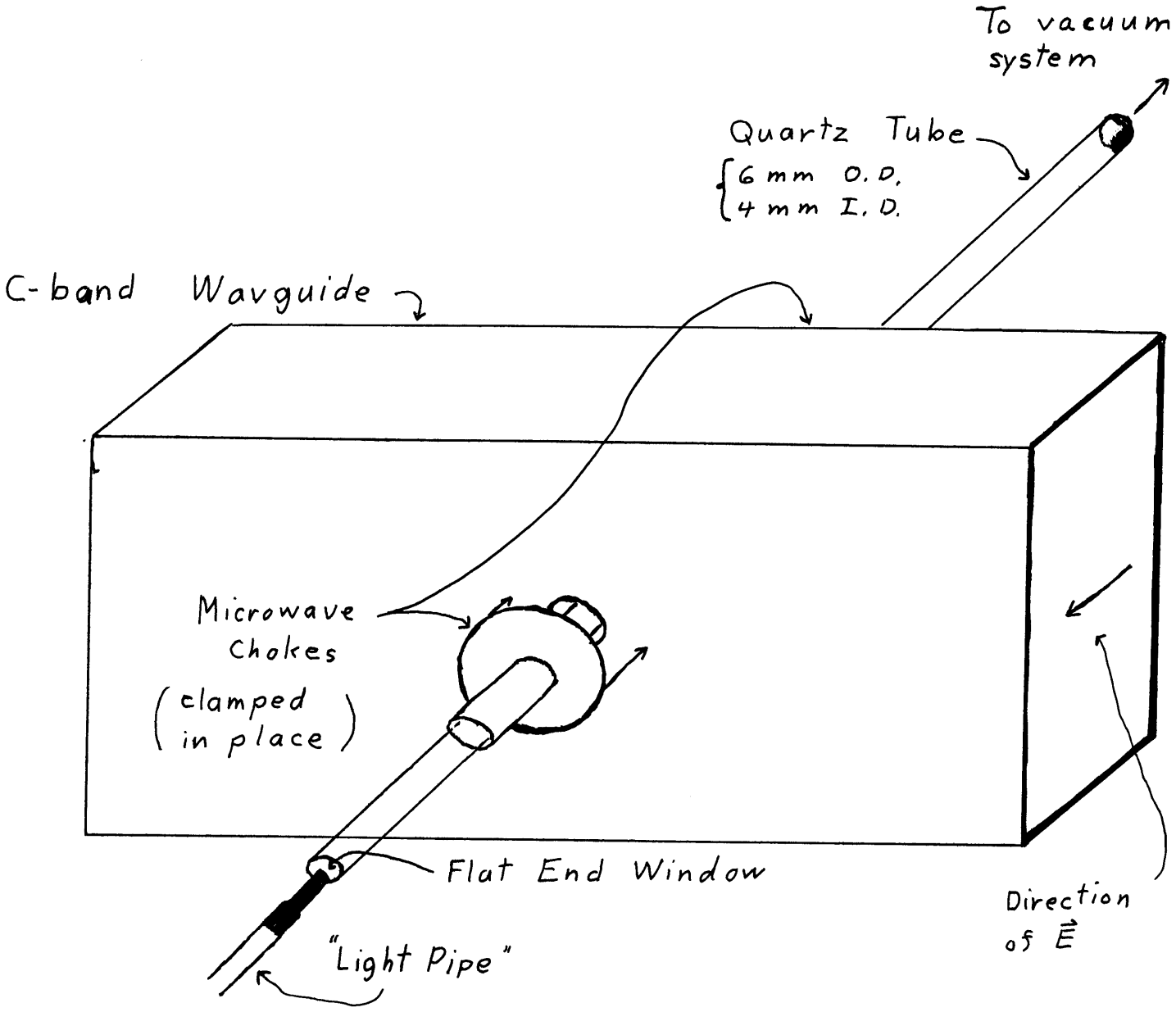

Cavity Discharge

Fig. 10

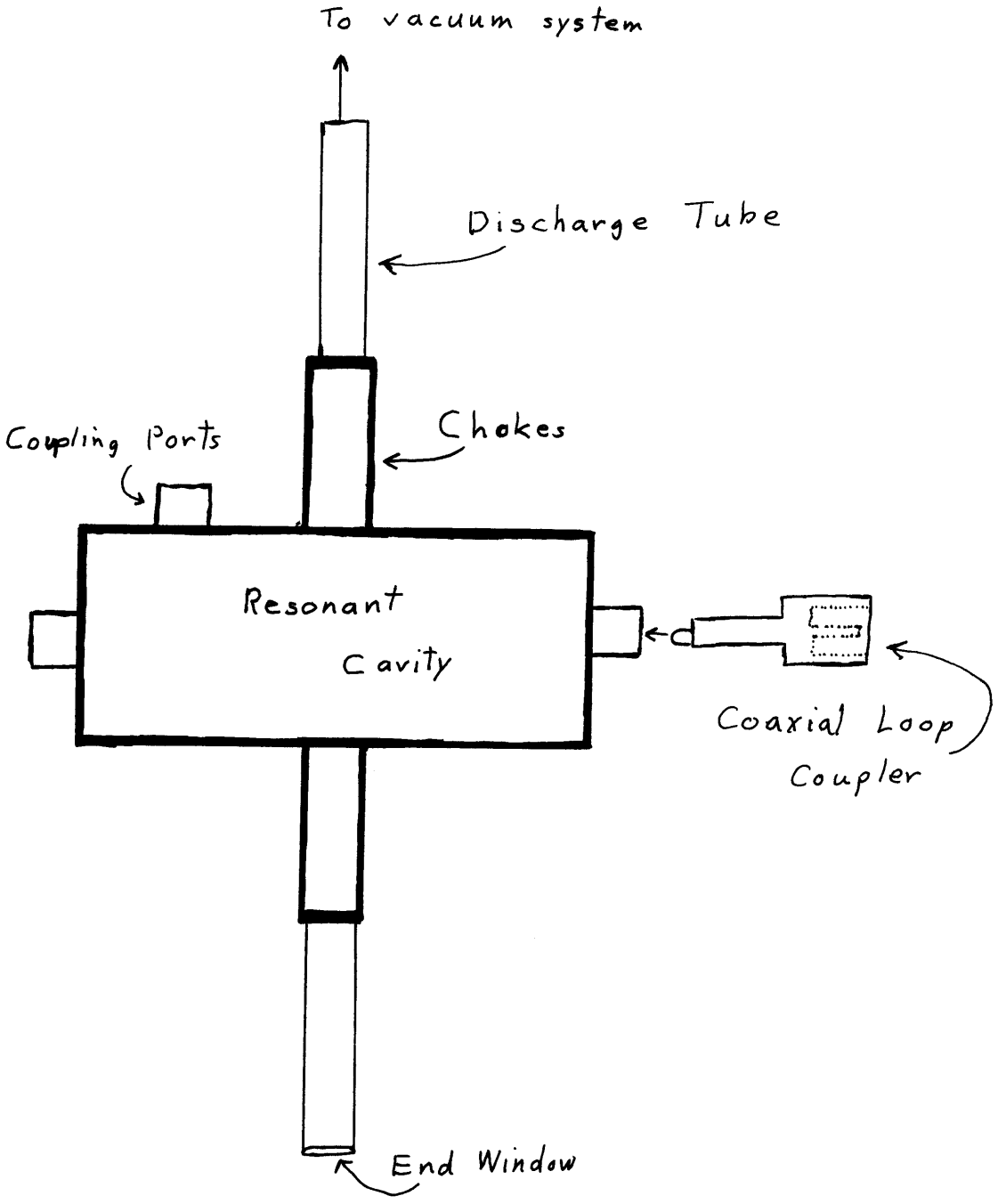

Microwave Driving Circuit

(Waveguide Discharge)

Fig. 11

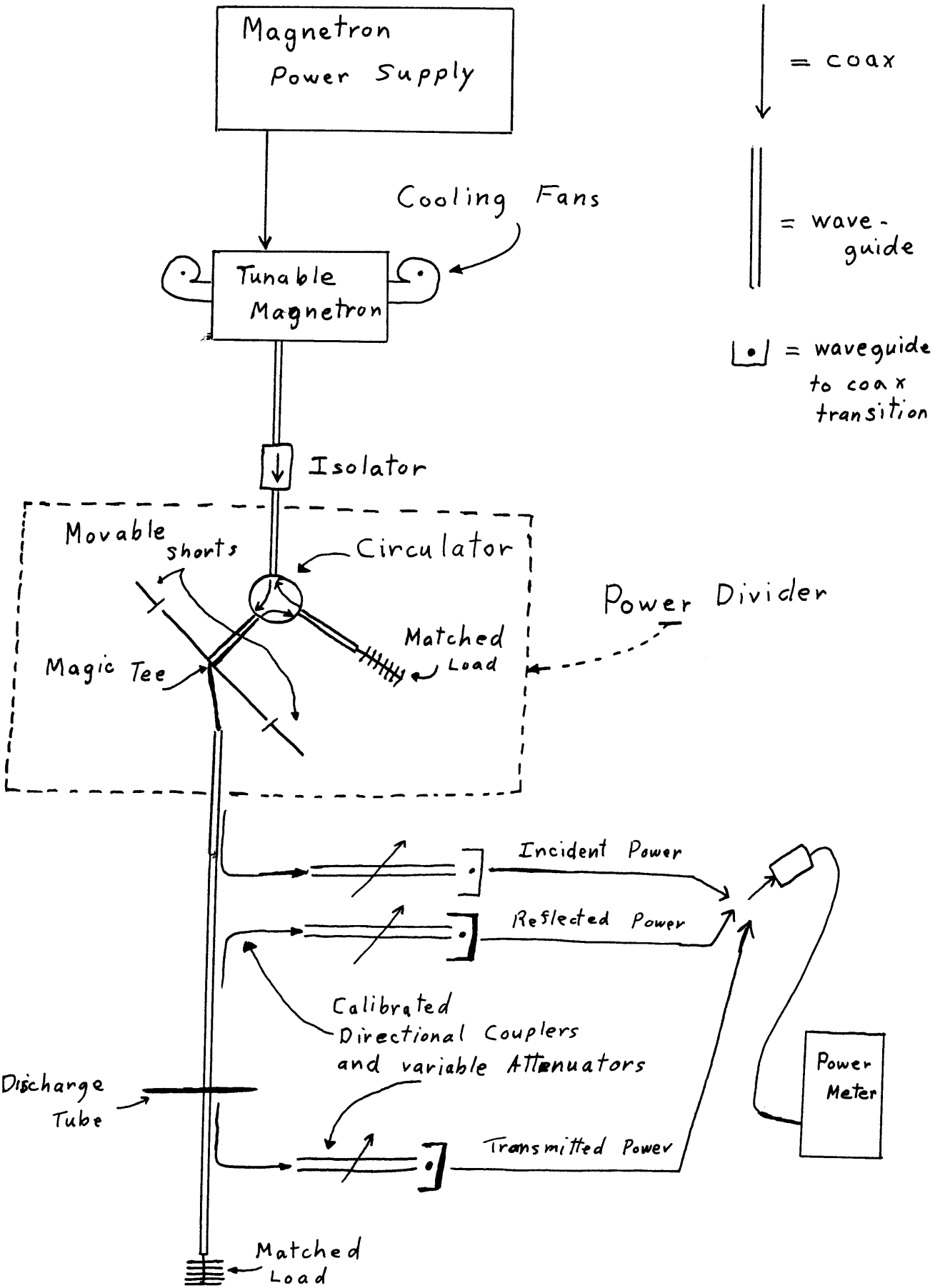

Microwave Driving Circuit Fig. 12

(Cavity Discharge)

Power Source Identical with Fig. 11

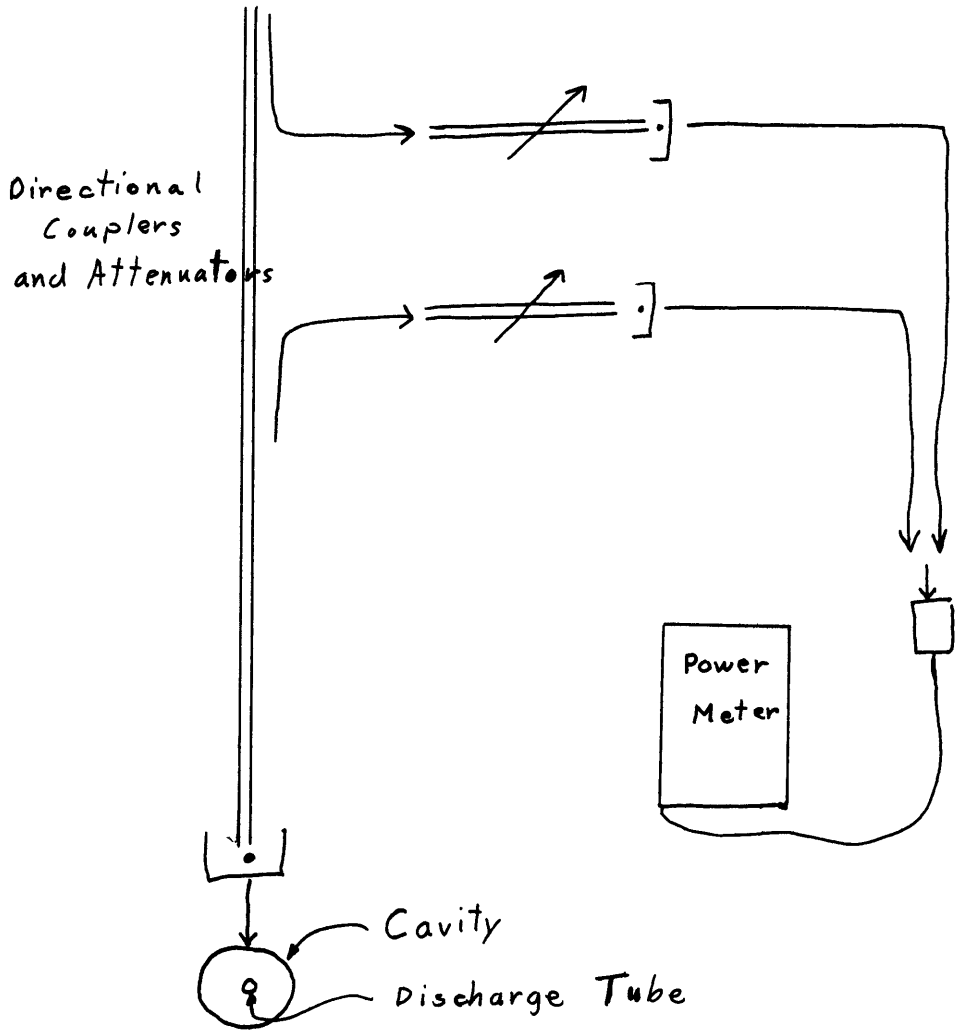

knowledge of the absolute power levels in the driving circuit and a measure of the power absorbed by the discharge would be available.

The cavity diagnostic circuit is shown in Fig. 13. The klystron reflector voltage is modulated by a sawtooth internally generated in the klystron power supply, thus sweeping the klystron frequency over a range of about 10 mc around a center frequency set by the tuning control on the klystron. This sawtooth is used to trigger the sweep of the oscilloscope which then displays the crystal voltage, as a function of the klystron frequency, on the vertical coordinate. The effective frequency response of the crystals was adjustable with the double stub tuners to the extent that it was possible to get a virtually flat response out of the crystals. The two crystals monitor the reflected power from the plasma cavity and the high Q cavity wave meter, and when these cavities absorb the reflected power is minimized and a pip appears on the oscilloscope display. If this pip is superimposed on the otherwise flat crystal response then any shift in the cavity frequency will shift the pip by a proportional amount on the oscilloscope display, thus allowing the calibration of the oscilloscope face in megacycles using the two cavity wave meter pips to mark two frequencies which could then be adjusted in distance apart so as to coincide with the

Diagnostic Circuit

Fig. 13

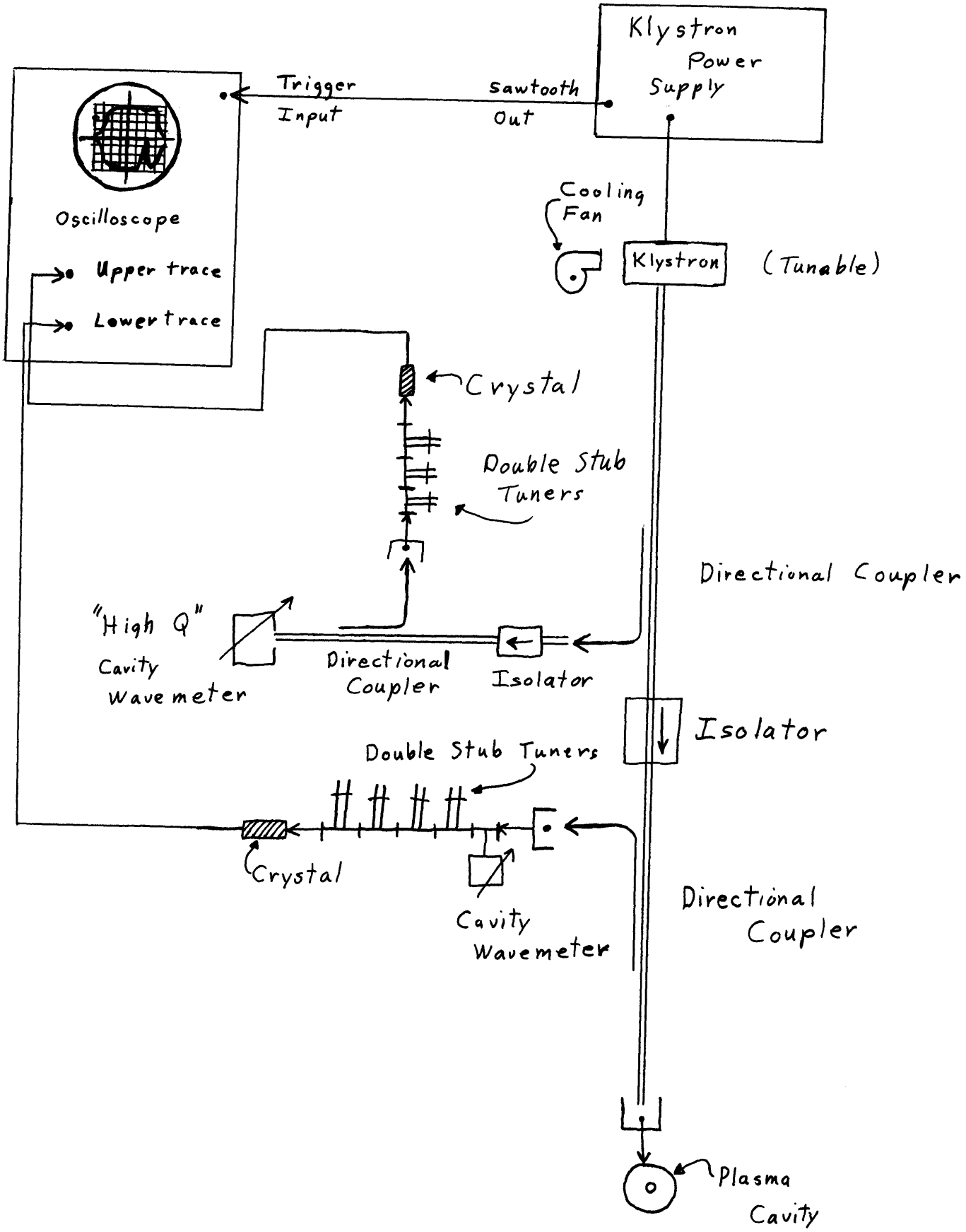

rulings on the oscilloscope display. Once the calibration was achieved the frequency shifts of the $TE_{0,1}$ mode as a function of plasma density were read directly from the oscilloscope face.

The light monitor circuit consists of an RCA 921 phototube in series with a 1 megohm resistor, powered by a 90 v battery, as shown below. The voltage across the resistor is then measured with a Hewlett-Packarge 410C voltmeter in order to determine the phototube current. The phototube is encased in a light tight box with a "light pipe" admitting the plasma light. The other end of the "light pipe" is placed flat against the flattened window at the end of the discharge tube, see Fig 9.

In order to use relatively pure He, the discharge tube was connected to a vacuum system and kept at a pressure of a few microns of Hg while not in use. The pressure of the gas was measured by observing the drop in height of the Hg column on the McLeod gauge which was attached to the vaccuum system from its height at the lowest pressure, before gas was admitted. The He was admitted from a tank and before each experiment the system was flushed several times with He, and then set at the desired pressure. Since the McLeod gauge was integral with the vacuum system and no traps were used there was

a significant Hg vapor content in the gas while running the discharge.

Using the above filling procedure, two experiments were done. The first was to observe the light intensity as measured by the H.P. 410C and measure the absorbed power for a waveguide discharge as a function of the incident power. The second was to measure the frequency shift of the TE_{011} mode of the cavity and the light intensity as the power incident on the discharge was varied, using the same light pickup geometry as in the waveguide discharge. For the cavity discharge it was necessary to wait unitl the cavity came the thermal equilibrium, due to heating of the cavity by the driving power. As the cavity heated the no-plasma TE_{011} frequency was observed to shift with time, finally coming to equilibrium. The results of these experiments and their interpretation are discussed in the following section.

Light Monitor

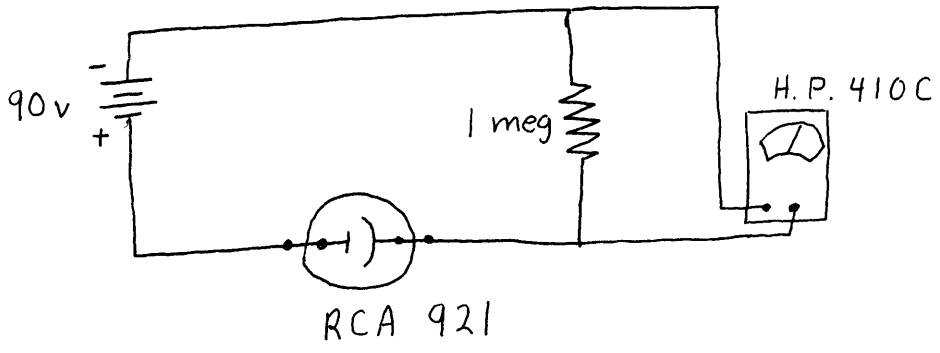

IV. The Experiment: Results and Interpretation

The behavior of the plasmas produced in these experiments seems to correlate well with the model of Ecker and Zöller. For the waveguide discharge it was found that the power absorbed by the discharge and the light intensity were both linear with the power incident. The cavity discharge produced a linear variation of the frequency shift with the light intensity as the incident power was varied. Some representative plots of these linear variations are given in Figs. 14,15, and 16. Due to the heating of the waveguide components connected to the cavity and the cavity itself it was impossible to determine accurately the power absorbed by the cavity discharge and thus the cavity experiments were restricted to the light intensity versus frequency shift studies. In the waveguide discharge it was found that as the incident power was decreased the discharge cut off at a higher power incident than for the cavity discharge, and thus the cavity light intensities go to lower values than those for the waveguide. Over a fairly wide range, however, the two light intensities are numerically comparable and linear with frequency shift and power incident for the waveguide and cavity discharges, respectively. Thus it is possible to set equal the densities

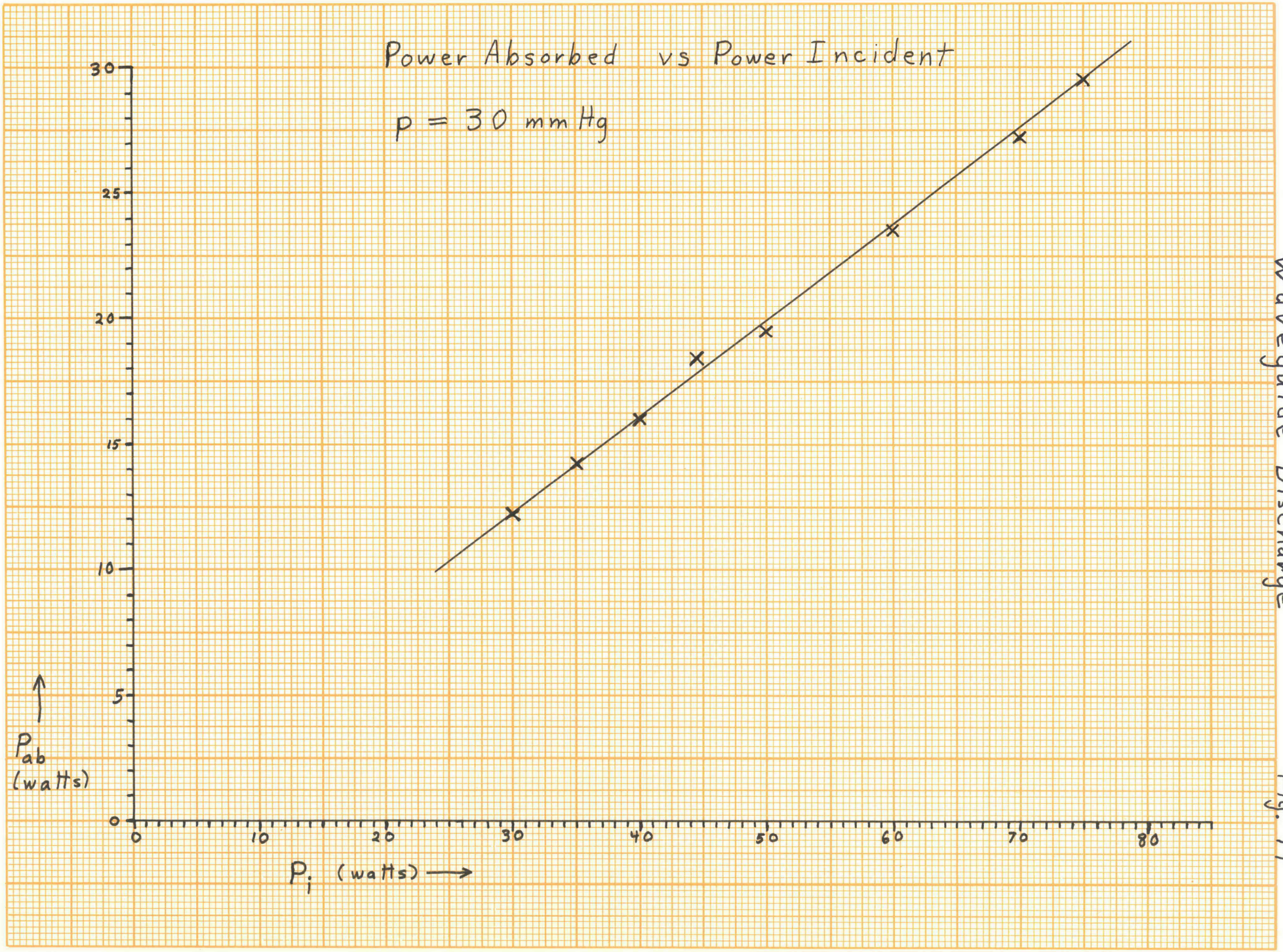

Waveguide Discharge

Fig. 14

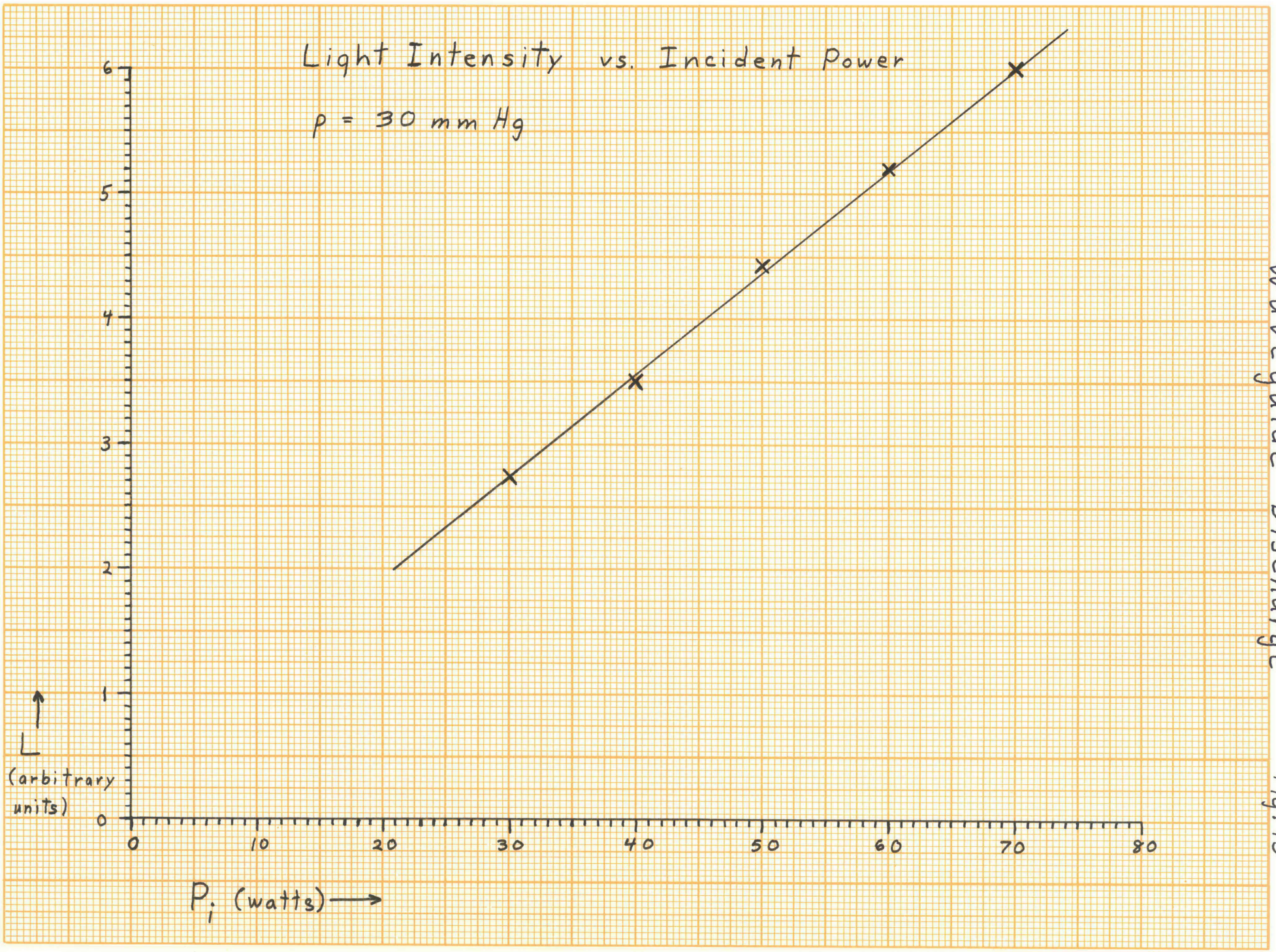

Waveguide Discharge

Fig. 15

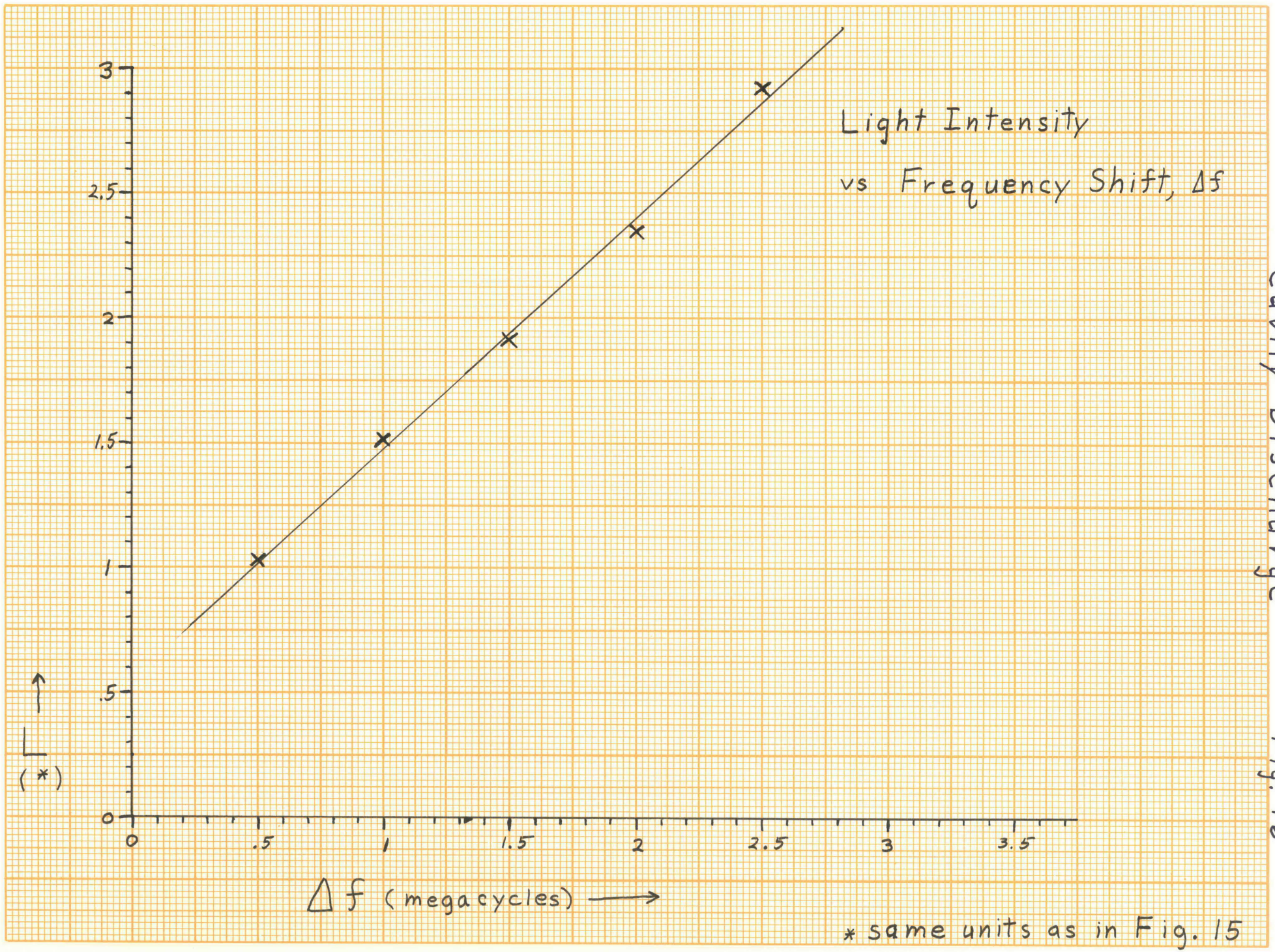

Cavity Discharge Fig. 16

in the cavity and the waveguide for the same light intensity, since the size of the discharge and the light measuring geometry were the same for both cases. Also, while the cavity discharge would "ignite" spontaneously for sufficiently high power levels, it was necessary to spark the waveguide mounted tube with a Tesla coil in order to start the discharge. The lower minimum power to run the cavity discharge is probably due to the fact that in the initial experiments the cooling fans on the magnetron set up an air current in the waveguide which then served to cool the discharge tube, while in the cavity there was virtually no air circulation. From equation [1] it is seen that a lower gas temperature implies a lower electron temperature for comparable electric field strength. When a thin sheet of mylar was introduced into the waveguide to stop the offending air flow the waveguide discharge was able to run at light intensity values comparable with the lower light values observed in the cavity discharge before it cut off as shown in Fig, 15. The unaided breakdown of the gas in the cavity discharge as opposed to the necessity of sparking the waveguide discharge is evidently a manifestation of the fact that for the same incident power level the cavity fields are much greater than the waveguide fields, which again correlates with equation [1] since for a higher E_o the energy balance implies a higher T_e for the same T_g.

The linear form of the absorbed power coupled with the roughly linear dependence of $n_{e,center}$ on P' (Fig. 2) would indicate that in the waveguide discharge the density is proportional to the incident power. The linear variation of light with frequency shift in the cavity and light with incident power in the waveguide are consistent with this if it can be assumed that the frequency shift is linear with electron density. For two reasons this assumption may not be valid. First the density profile may be changing significantly as the power increases, and, second, the gas temperature may be changing with absorbed power. Both of these variations are expected from Ecker and Zöller's treatment. The density profile change may not be important insofar as Ecker and Zöller's treatment indicates that as the profile begins to flatten its shape changes less drastically with increasing power absorbed. From equation [18] the gas temperature variation may also play a less than catastrophic role if the wall temperature does not change drastically. While these effects should be checked further, possibly by monitoring the wall temperature of the discharge tube or devising a way to keep it constant and by devising an independent method of determining the density profile, it is not clear that they necessarily change the linear variation of density with frequency shift to a

significant degree.

The linear variation of the power absorbed, P_{ab}, with the power incident, P_i, is found to be reasonably consistent with the two solutions of the wave equation previously derived. This is seen from the following argument.

From the experiment (Fig. 14), $\overline{P}_{ab} = k_o \overline{P}_i$; from the treatment of Ecker and Zoller, $\Delta T = c_o \overline{P}_{ab}$ and $\overline{P}_{ab} = c_1 n_{e,c}$. Thus $\Delta T = c_o c_1 n_{c,c} = k_1 \overline{P}_i$. Now the time average power absorbed, $\overline{P}_{ab}$, is simply:

$$[19] \quad \overline{P}_{ab} = \int_{V_{plasma}} \overline{\vec{J} \cdot \vec{E}} \, dv = \frac{1}{2} \int_{V_p} \frac{\omega_p^2(r) \, \nu_m(r) \, E_p^2}{\nu_m^2(r) + \omega^2} \, dv$$

where the r dependence of ν_m comes from the r dependence of T_g since $\nu_m = c T_g^{-1}$. Thus $\nu_m(r) = c\left[\Delta T \, t(r) + T_{g,wall}\right]^{-1}$ since we can set $T_g(r) = \Delta T t(r) + T_{g,w}$ where $t(0) = 1$ and $t(R) = 0$ and $t(r)$ assumes the proper shape required by Ecker and Zoller. Likewise, $\omega_p^2(r) = n_{e,c} \, s(r)$. Now if $E_p^2/E_o^2 = g\left(\frac{\omega_p^2(n_{e,c})}{\nu_{m,c}^2 + \omega^2}\right)$, where E_p is the (constant) field within the plasma; then equation [19] can determine the required form for $g\left(\frac{\omega_p^2(n_{e,c})}{\nu_{m,c}^2 + \omega^2}\right)$ to satisfy the experiment and the treatment of Ecker and Zoller. Now equation [19] becomes

$$k_o \overline{P}_i = \frac{1}{2} g c_2 \overline{P}_i \int_{V_p} \frac{\omega_p^2(r) \, \nu_m(r)}{\nu_m^2(r) + \omega^2} \, dv$$

since E_o^2 can be written $c_2 \bar{P}_i$. In the range of parameters of interest here $\nu_{m,wall}^2$ can be taken a much greater than ω^2 if ω is the frequency of the driving field. Thus:

$$k_o \doteq \frac{c_2 g}{2c} \int_{V_p} n_{c,e}\, s(r) \left[\Delta T\, t(r) + T_{g,w}\right] dv$$

$$\text{or,} \qquad g = \frac{1}{n_{e,c}} \cdot \frac{2 k_o c}{c_2} \left[\int_{V_p} s(r) \left[c_o c, n_{e,c}\, t(r) + T_{g,w}\right] dv\right]^{-1}$$

This form is reasonably consistent with the $\left[\omega_{po}^2 / (\nu_{m,c}^2 + \omega^2)\right]^{-1}$ dependence exhibited by Fig. 7 and 8 at least insofar as the term under the integral sign is not a sensitive function of density, and if the $\nu_{m,c}^2$ term in $\omega_{po}^2 / (\nu_{m,c}^2 + \omega^2)$ can be said to remain constant or vary slowly with $n_{e,c}$. These conditions will certainly hold for the low temperature limit when $\Delta T << T_w$ and $\nu_m(r)$ is then virtually constant; the behavior of these terms at higher densities and temperature is not clear but some deviation from the $\left[\omega_{po}^2 / (\nu_{m,c}^2 + \omega^2)\right]^{-1}$ dependence will certainly occur.

Thus it would seem that the gross approximations made in handling the wave equation do not mask the crucial properties of the behavior of g which are required for consistency with the treatment of Ecker and Zoller and that a more careful theoretical treatment of the wave equation along these lines might be more fruitful.

On all counts, then, the qualitative aspects of the plasmas produced in these experiments indicate that the basic concepts of the theory used here should be capable of describing the steady state microwave discharge variation of electron density with incident power if a more rigorous treatment can be constructed.

In order to indicate the orders of magnitude involved Fig. 17 shows a derived plot of $n_{e,c}$ as a function of P_i using the density measured in the cavity, assuming equation [18] to be valid, to give the density in the waveguide at two points of comparable light intensity for both discharges and then using the number $k' = \frac{\Delta P_i \text{ (measured in the waveguide)}}{\Delta n_{e,c} \text{ (measured in the cavity)}}$ to set the slope of the line. As indicated $n_{e,c}$ is calculated for a Bessel function and a uniform profile.

Fig. 17

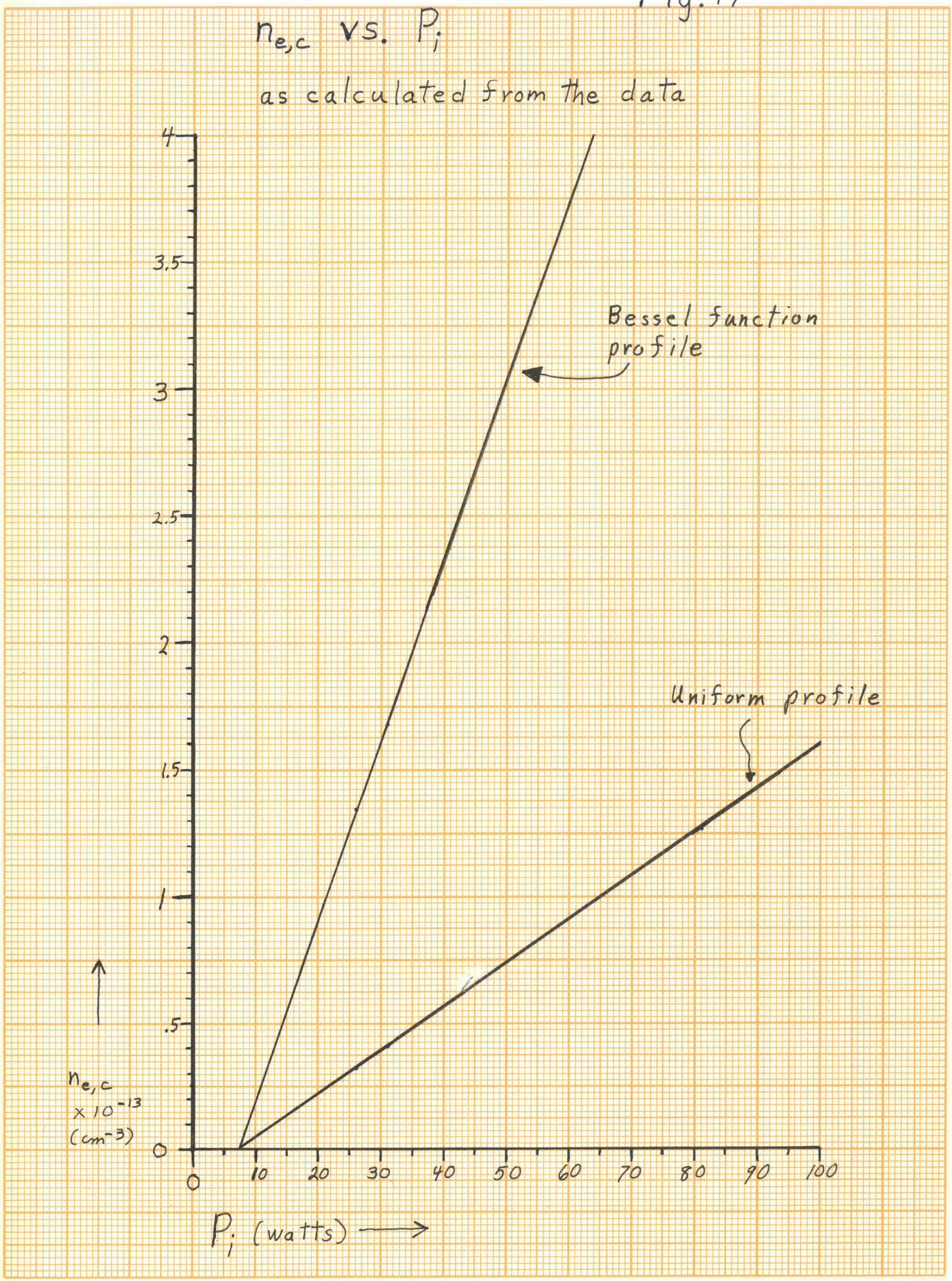

B I B L I O G R A P H Y

1. S. C. Brown, Introduction to Electrical Discharge in Gases, John Wiley and Sons, Inc., New York, 1966.
2. D. J. Rose, S. C. Brown, Phys. Rev. 98, 310 (1955)
3. W. P. Allis, D. J. Rose, Phys. Rev. 93, 84 (1954)
4. W. P. Allis. S. C. Brown, E. Everhart, Phys. Rev. 84, 519 (1951)
5. J. C. Ingraham, Private Communication
6. W. P. Allis, Research Laboratory of Electronics, Technical Report, 299, M.I.T. 1956.
7. G. Ecker, O. Zöller, Physics of Fluids, Vol. 7, Number 12, p. 1996, (1964).
8. M.A. Heald, C. B. Wharton, Plasma Diagnostics with Microwaves, John Wiley and Sons, New York, 1965.
9. S. J. Buchsbaum, Interaction of Electromagnetic Radiation with a High Density Plasma, Doctoral Thesis, Massachusetts Institute of Technology, 1957.
10. J. C. Ingraham, S. C. Brown, Plasma Diagnostics, Research Laboratory of Electronics, Technical Report 454, Massachusetts Institute of Technology, 1966.